THE EFFECT OF OFFSET RATIO ON THE MEAN FLOW CHARACTERISTICS OF TURBULENT OFFSET JETS

A. Nasr and J.C.S. Lai

School of Aerospace & Mechanical Engineering
University College, The University of New South Wales
Australian Defence Force Academy, Canberra 2600, AUSTRALIA.

ABSTRACT

Two-dimensional offset jets have been studied extensively because of their significance in engineering applications. However, previous studies have been mainly focussed on jets with relatively high offset ratios and have been mainly concerned with the determination of attachment lengths through static pressure measurements or flow visualisation techniques. There has only been one study in the literature that involves LDA measurements of the mean velocity field. In this investigation, the velocity field of two-dimensional offset jets with relatively low offset ratios, namely, 2.125, 5.125 and 7.5, has been measured using a two-component laser Doppler anemometer. Wall static pressure measurements indicate that three-dimensional effects cannot be neglected unless side plates are installed. The static pressure gradient (and hence the curvature of the jet attaching to the wall) decreases with increasing offset ratio. It has been shown that the differences between attachment lengths determined from the mean velocity vector field and the locations of maximum static wall pressure are within a few percent of each other. The attachment length increases with increasing offset ratio according to an approximately 4/5th power law. Although mean streamwise velocity profiles when appropriately nondimensionalised collapse very well at the attachment point, no such collapse can be effected for profiles of turbulence quantities.

NOMENCLATURE

b	averaged jet half-width = $0.5(b_+ + b_-)$
b_+	jet half-width in the outer shear layer of offset jets (Fig. 1).
b_-	jet width in the inner shear layer of offset jets (Fig. 1).
P	static pressure relative to atmospheric pressure
P_0	stagnation pressure in the settling chamber relative to atmospheric pressure
P_∞	atmospheric pressure
Re	Reynolds number, $U_0 w/\nu$
U	mean streamwise velocity
U_m	local maximum streamwise velocity
U_0	mean streamwise velocity at the nozzle exit
u',v',w'	rms of velocity fluctuations in x, y and z (normal to the x-y plane) respectively
$\overline{uv}$	Reynolds shear stress
V	mean lateral velocity
x,y,z	streamwise, lateral, and normal coordinates in a Cartesian coordinate system (Fig.1)
x_{ip}	attachment length (measured along the wall from the nozzle plate)
x_{maxp}	streamwise distance of the location of maximum wall static pressure
x_{vc}, y_{vc}	streamwise and lateral coordinates of the standing vortex centre
$y_{1/2}$	lateral location of jet half-width in the outer shear layer (Fig. 1)
$y_{-1/2}$	lateral location of jet half-width in the inner shear layer (Fig. 1)

INTRODUCTION

The flow field of an offset jet is complex and is encountered in many engineering applications. For instances, burners, boilers, gas turbine combustion chambers, and fuel injection systems are strongly governed by the behaviour of offset jets. Fundamental study of the flow field of offset jets can also lead to better understanding of similar flows such as backward-facing step flows and sudden expansion flows.

Various features of an offset jet flow are shown schematically in Fig. 1. Here the Cartesian coordinate system (x-y) is set so that its origin is at the intersection of the nozzle plate and the wall and the x-axis is along the wall. A plane, incompressible, turbulent air jet is discharged from a plane nozzle with width w into quiescent ambient surroundings above a wall offset by a distance h and parallel to the axis of the jet discharge.

Entrainment of the air bounded by the jet and the offset wall causes a sub-atmospheric pressure zone, resulting in the jet being deflected towards the wall in the converging region and eventually attached to it at the impingement point (ip), also referred to as the attachment or reattachment point in the literature. Part of the inner shear layer fluid is deflected upstream from the attachment point into the recirculation zone by an adverse pressure gradient. Downstream from the attachment point, in the attachment region, the flow is subjected to the effects of stabilising curvature, adverse pressure gradient and the strong interaction with the offset wall. Far downstream from the nozzle plate, in the wall jet region, the flow continues to develop to resemble a wall jet flow.

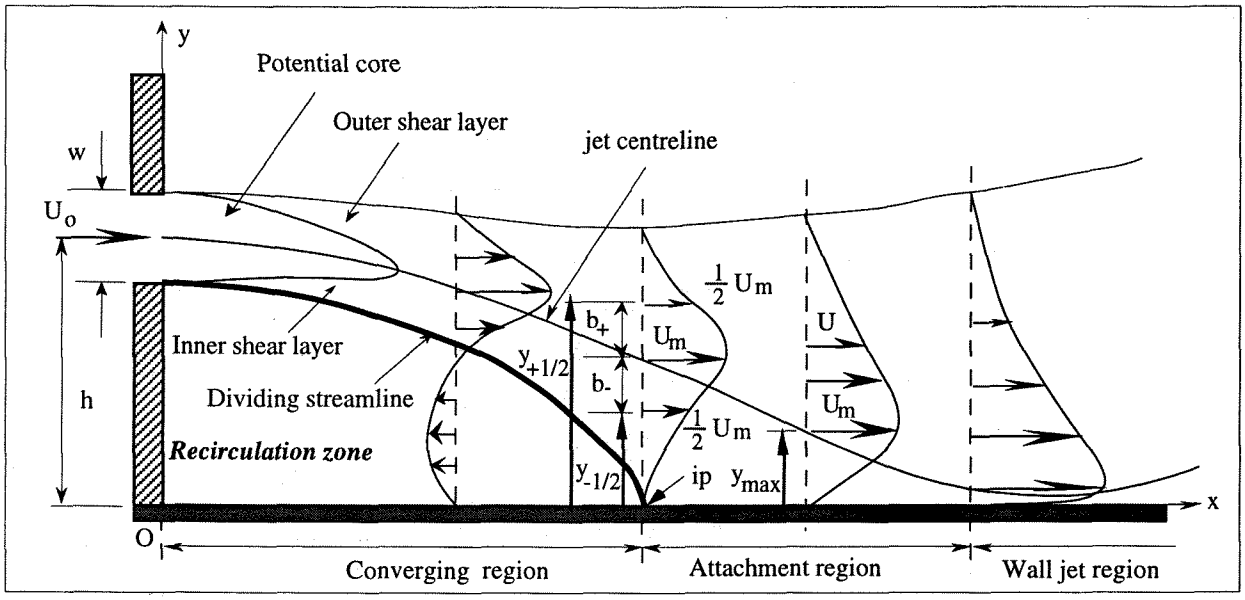

Fig. 1 Schematic diagram of an offset jet.

There have been many experimental investigations on two-dimensional reattaching offset jet such as Bourque and Newman [1], Newman [2], Sawyer [3,4], Bourque [5], McRee & Moses [6], Perry [7], Rajaratnam & Subramanya [8], Ayukawa and Shakouchi [9], and Nozaki et al. [10], Hoch and Jiji [11], Nozaki et al. [12] and Lund [13]. These studies included the measurements of static pressure distributions, mean streamline velocity profiles, and the effect of offset ratio on the streamwise distance of the attachment point from the nozzle plate (x_{ip}) for jets with offset ratios from 0.694 to 48. Nonetheless, there are numerous discrepancies among reported experimental results. For instance, early studies of Bourque and Newman [1] and Sawyer [3,4] had assumed an uniform pressure within the recirculation zone and hence a constant radius of curvature of the jet centre line which was examined by Bourque [5] and Rajaratnam & Subramanya [9] to be erroneous. The reasons for discrepancies in the experimental results reported in the literature for offset jet might be due to different nozzle exit conditions such as nozzle exit Reynolds number, initial turbulence intensity, static pressure gradient at nozzle exit, nozzle aspect ratio and different experimental techniques.

Previous investigations have been focussed on jets with relatively high offset ratios. Studies of low offset ratios were mainly concerned with static pressure measurements in determining attachment lengths. With the exception of Pelfrey & Liburdy [14], previous measurements were made with hot-wires or Pitot tube which cannot discriminate against reversed flow in the recirculation flow region . Pelfrey & Liburdy [14] used two component laser Doppler anemometer to measure velocity components and turbulence intensities of an offset jet with an offset ratio of 7 at a nozzle exit Reynolds number of 15,000. They found that the magnitude of the curvature strain rate is significant, thus implying that the flow field cannot be accurately modelled as a thin shear layer.

The objectives of the work reported in this paper, were, therefore,

- to measure the velocity field of two-dimensional turbulent offset jets with relatively small offset ratios, namely 2.125, 5.125 and 7.5 using laser Doppler anemometry;
- to determine the attachment length from mean velocity measurements and wall static pressure measurements; and
- to document the flow characteristics of these three offset jets as a database for turbulence modelling.

APPARATUS AND INSTRUMENTATION

Apparatus

The two-dimensional jet rig, shown schematically in Fig. 2, is similar to that previously used by Nasr [15]. The perspex jet settling chamber is 770 mm long, 150 mm wide and 400 mm high. The air flow rate was controlled with a frequency invertor (KVFN 222H

Transistor Invertor manufactured by KASUGA E. W. Ltd. Japan) in conjunction with a butterfly valve at the blower inlet, giving various nozzle exit velocities up to 50 m/s. Grids were used in the settling chamber to reduce the nozzle exit turbulence intensity. The turbulence intensity on the centreline at the nozzle exit is less than 2%. A two-dimensional nozzle with nozzle width (w) of 6 mm and an aspect ratio of 30 was made of aluminium plate. The length of the offset wall was 200 mm, approximately 34w. The nozzle plate thickness was 7.5 mm and the nozzle inlet profile consisted of a relatively short inner smooth section with a straight conduit of 6 mm. Side plates (250 mm x 200 mm) were placed horizontally at the top (ceiling) and bottom (floor) sides of the nozzle in order to enhance two-dimensionality of the flow by preventing air entrainment through the top and bottom sides of the jet.

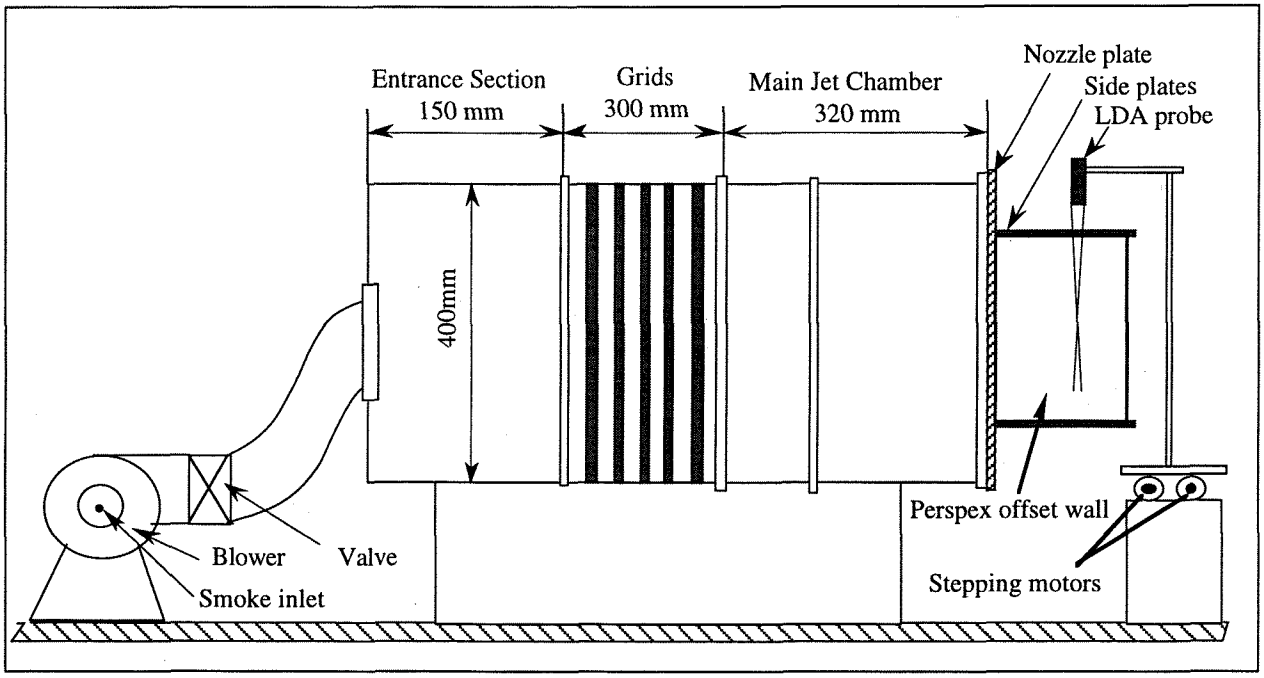

Fig. 2 Schematic diagram of the experimental rig.

The LDA and pressure probes were traversed in x and y directions by two stepping motors controlled by an *NEC* 286 computer. The smallest step in each direction was 0.015 mm. A smoke generator, SMT 1482 Smoke Tunnel (manufactured by Plint & Partners Ltd. England) was used for seeding the flow for LDA measurements. The liquid used to produce smoke was non-poisonous Rosco " FOG FLUID " made by Rosco Laboratories INC., USA. Seeding particles (smoke) were introduced into the flow at the inlet of the blower for LDA measurements.

Instrumentation

The LDA system comprised a Coherent's INNOVA 70 series Ar-ion laser and two DANTEC 57N10 Burst Spectrum Analysers (BSA) Each BSA was set to eliminate signals out of the frequency band of interest in order to maximise the signal-to–noise ratio of the Doppler signals. Good quality signals were then detected through a burst detector unit. The burst detector could operate on either the pedestal of the Doppler burst, the envelope of the band-pass filtered or a gated version of the two detector signals. Four data collection modes namely burst, continuous, dead time and external modes were available in the Burst Spectrum Analyser. In this study, because of the need to measure both transit and arrival times of particles, and to apply amplitude discrimination, the burst mode of data acquisition was preferred. Detailed description of the BSA circuitry can be found in the BSA manual BURSTware 2.00[16].

BURSTware application program version 2.00, which was designed for Dantec Burst Spectrum Analyser-based laser Doppler anemometry (LDA), was used for both signal acquisition and data processing. The number of burst samples for each measurement was set at 3000 and raw data was processed by applying residence time weighting function to eliminate velocity bias errors. LDA results were validated by theoretical results and hot wire data made in a single free jet at 24 nozzle widths downstream from the nozzle plate [15].

Analysis of the LDA data showed that the uncertainties in the measured mean velocities (U, V), rms velocity fluctuations (u', v'), and velocity correlation $\overline{uv}$ are within ± 0.085 m/sec, ± 0.09 m/sec and ± 0.4 m^2/sec^2 respectively.

Disc type static pressure probe

As a standard static pressure probe is very sensitive to the flow direction, it is subject to severe errors in flow fields that involve high streamline curvature such as in the converging region and recirculation zone of offset jets. Therefore, a disc type static pressure probe was designed in this study. The dimensions of this probe are given in Fig. 3. This probe was used in conjunction with an MKS type 398 differential pressure transducer and an MKS type 270B display unit to acquire static pressure data.

The polished surfaces of the disc type static pressure probe were aligned accurately in the plane of measurements (x-y plane) to minimise the effects of the streamwise and lateral turbulence intensities on the pressure readings. The probe was validated against a standard Pitot-static tube in the test section of a low turbulence subsonic wind tunnel. All pressure measurements were made relative to a reference tap exposed to stagnant atmosphere far from the jets.

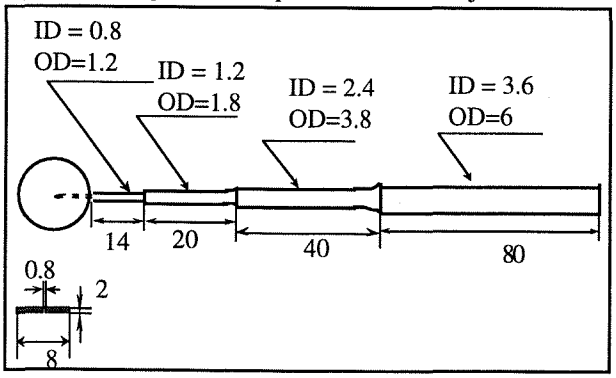

Fig. 3 Schematic diagram of the disc type static pressure probe (dimensions in mm).

RESULTS AND DISCUSSIONS

LDA measurements were made for two-dimensional offset jets with offset ratios 2.125, 5.125 and 7.5 for streamwise distances up to 20 nozzle widths downstream. The nozzle exit velocity for each jet was 26.5 m/s, giving a nozzle exit Reynolds number of 11,000.

Effect of side plates

Fig. 4(a) shows the normalised static gauge pressure along the wall with and without the installation of side plates for the offset jet with h/w=2.125. It can be seen that for both cases, the wall static pressure immediately downstream of the nozzle is subatmospheric, stays approximately constant for about 3 nozzle widths, then increases sharply to a maximum above atmospheric at some distance downstream. However, in the absence of side plates, as a result of entrainment of the surrounding air through the top (ceiling) and the bottom (floor) sides of the jet, the static pressure in the recirculation region bounded by the nozzle plate, the wall and the inner shear layer of the jet is higher than that with side plates installed. This would imply that the jet without side plates will curve at a lower rate towards the wall than that with side plates. Furthermore, the maximum static pressure attained by the flow after attachment to the wall is higher when side plates are installed. Kumada et al [17] and Sawyer [3] used the point of maximum static pressure to identify the attachment point. Fig. 4(a) indicates that the maximum static pressure for the jet with and without side plates occurs at x_{pmax}/w=4.75 and 6.25 respectively.

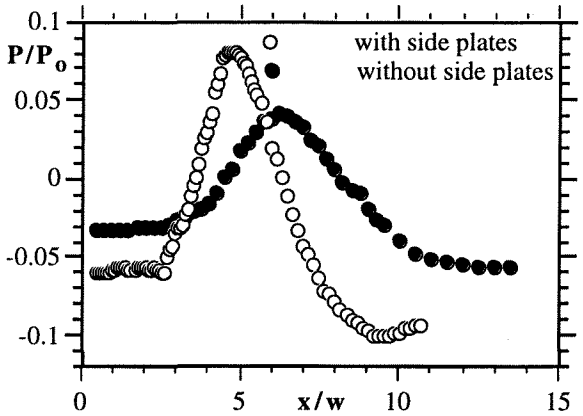

Fig.4(a) Effect of side plates on the wall static pressure (h/w=2.125).

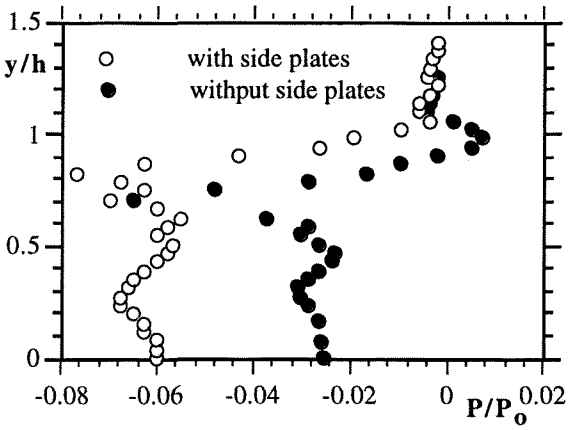

Fig. 4(b) Effect of side plates on the lateral distribution of static pressure at x/w=0.5 (h/w=2.125).

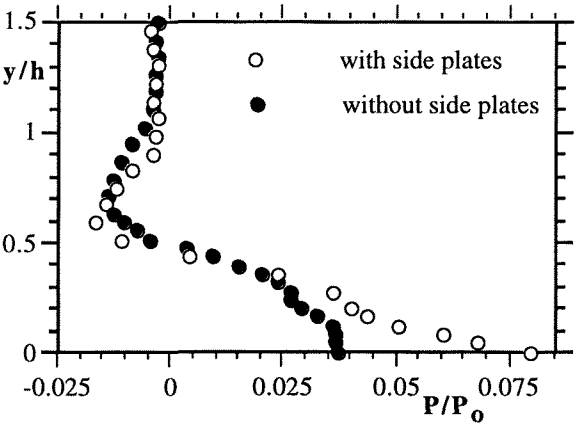

Fig. 4(c) Effect of side plates on lateral distribution of static pressure at attachment point (ip) (h/w=2.125).

Fig. 4(b) shows the effect of side plates on the lateral distribution of the normalised static gauge pressure at x/w=0.5. It can be seen that except near the edge of the jet, the static pressure is subatmospheric with and without side plates. However, the static pressure with side plates installed is substantially lower than that without side plates, thus leading to faster and stronger deflection of the jet towards the wall. Consequently, the jet without side plates should attach to the wall further downstream than that with side plates installed, as has already been observed in Fig. 6(a). Hence, for investigations of two-dimensional offset jets, side plates have to be installed to reduce three-dimensional effects. At the attachment point, the lateral distribution of normalised static gauge pressure with and without side plates is very similar to each other except near the wall (Fig. 4(c)).

Effect of Reynolds number

Fig. 5 shows the normalised static gauge pressure along the wall for h/w=2.125 for Reynolds number in the range 3300 - 15200. It can be seen that while the static pressure distribution is dependent on the Reynolds number for Reynolds number less than 11000, the static pressure distributions for Re=11000 and 15200 are almost indistinguishable from each other. Furthermore, the static pressure distribution for Re=7400 is already approaching that of Re=11000. Hence, for sufficiently large Reynolds number (in this case, greater than 10,000), the static pressure distribution is virtually independent of Reynolds number. These observations are consistent with the results of Bourque & Newman [1].

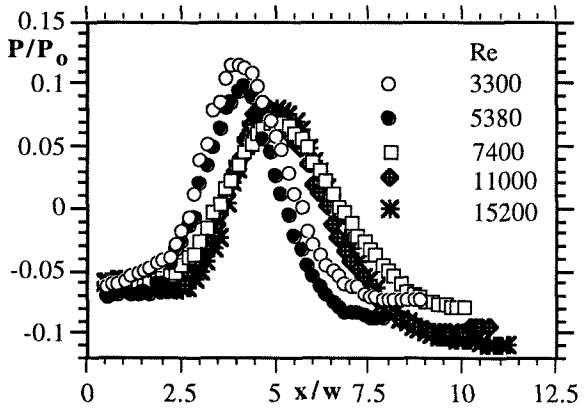

Fig. 5 Effect of Re on distribution of wall static pressure (h/w=2.125).

Static pressure measurements

The normalised static gauge pressure along the wall for the three offset jets is shown in Fig. 6(a). Maximum static pressure for h/w=2.125, 5.125 and 7.5 occurs at x_{pmax}/w=4.7, 13.8 and 17.1 respectively. Kumada et al [17] stated that the values of maximum and minimum static pressure remain essentially constant for offset ratios between 2 and 6 and decrease with offset ratio for offset ratio greater than 6. However, Fig. 6(a) indicates that the magnitude for minimum static pressure decreases as the offset ratio increases, thus implying that there is a much stronger lateral pressure gradient and hence stronger deflection of the jet towards the wall at lower offset ratio.

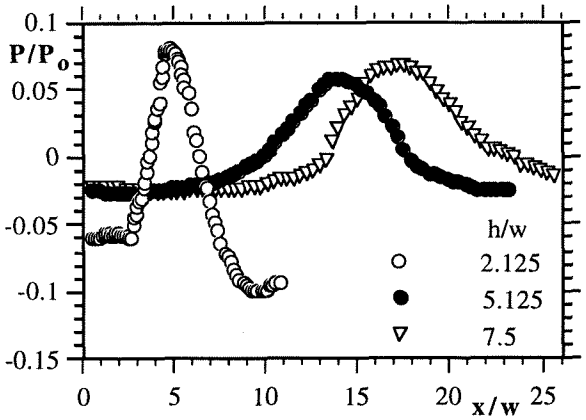

Fig. 6(a) Wall static pressure distributions for various offset ratios.

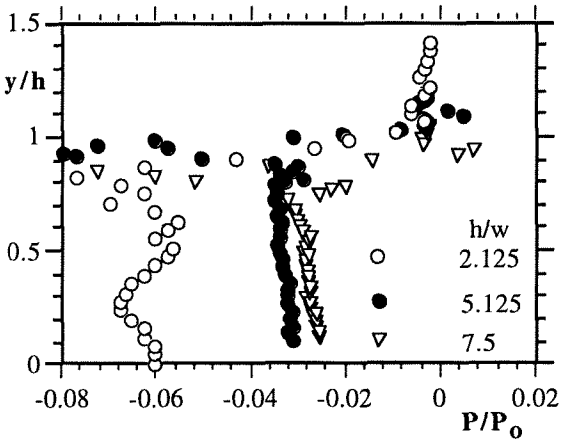

Fig. 6(b) Static pressure profiles at x/w=0.5 for various offset ratios.

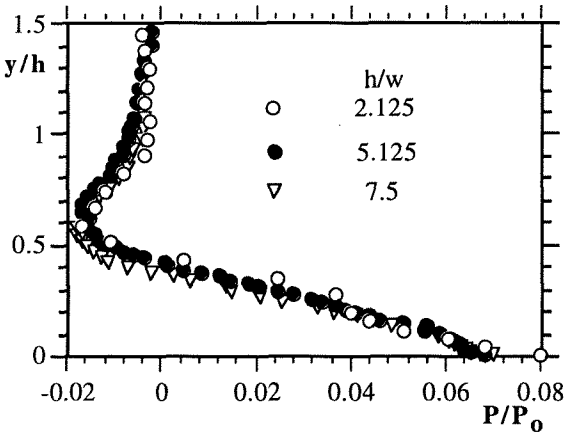

Fig. 6(c) Static pressure profiles at attachment point (ip) for various offset ratios.

The static pressure profiles at x/w=0.5 near the nozzle exit in Fig. 6(b) clearly indicate that except near the edge of the jet, the static pressure is subatmospheric for all three offset jets with the lowest value for h/w=2.25

and highest for h/w=7.5. These results are consistent with the observations made in Fig. 6(a). The normalised static pressure profiles at x_{ip} (determined from measured mean velocity vectors) in Fig. 6(c) show that when the lateral coordinate (y) is nondimensionalised by the offset distance (h), they are virtually independent of the offset ratio.

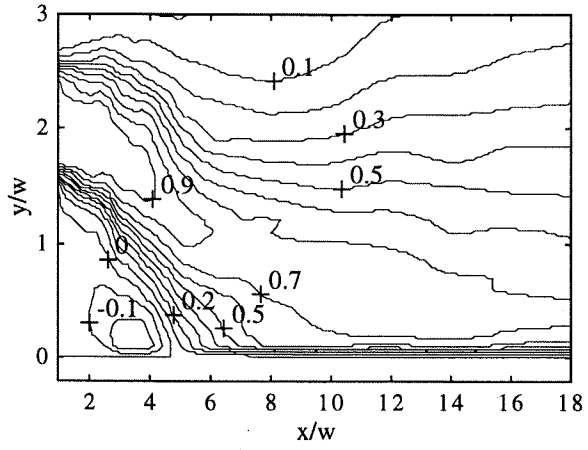

(a) h/w=2.125

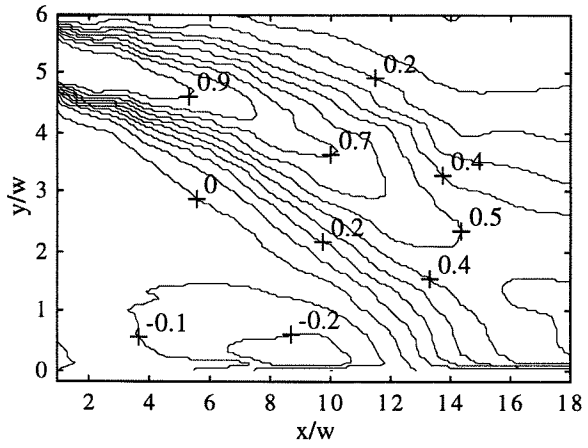

(b) h/w=5.125

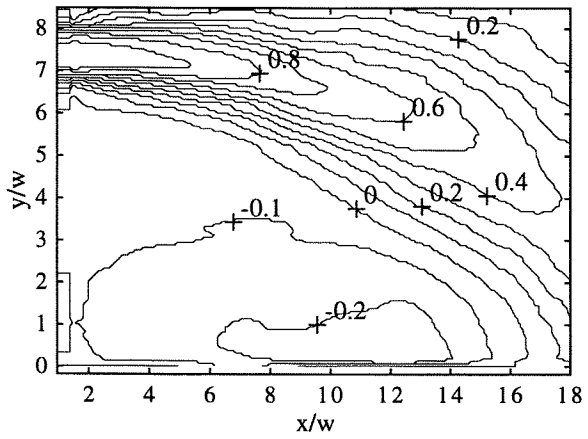

(c) h/w=2.125

Fig. 7 Contours of mean streamwise velocities.

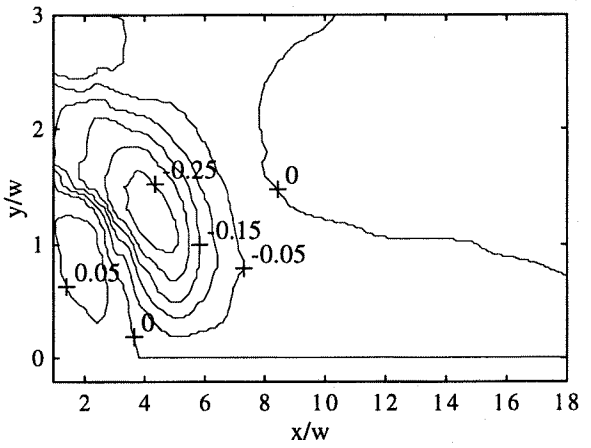

(a) h/w=2.125

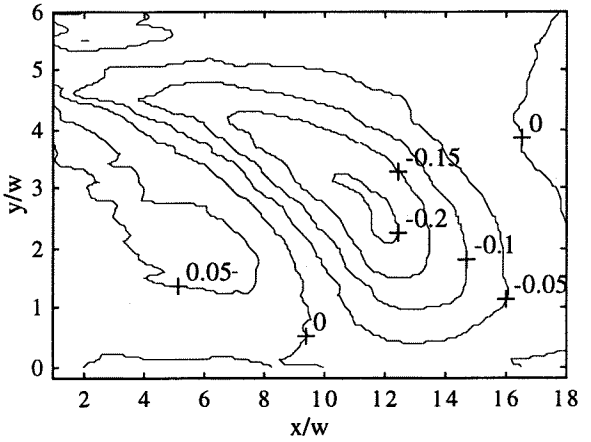

(b) h/w=5.125

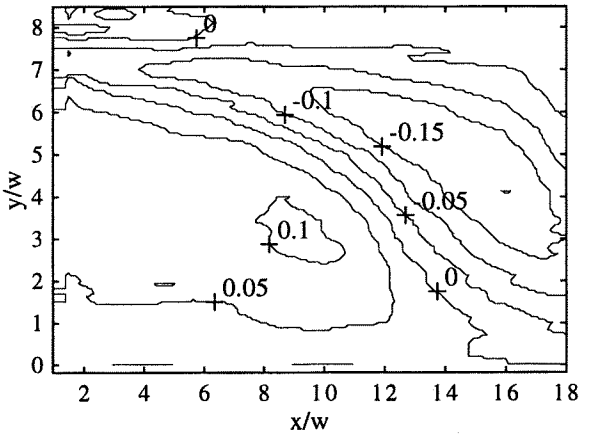

(c) h/w=2.125

Fig. 8 Contours of mean lateral velocities.

Mean velocity field

Contours of mean streamwise velocities for the three offset jets are given in Fig. 7. For each offset ratio, it is evident that the jet starts deflecting towards the wall as soon as it leaves the nozzle. Contours of negative mean lateral velocities which indicate the flow towards the wall, can be identified in Fig. 8. It can be seen that the magnitude of maximum negative lateral velocity decreases with offset ratio, thus indicating that the lateral static

pressure gradient is largest for h/w= 2.125, as has already been observed in Fig. 8. The magnitude of maximum negative lateral velocity for h/w=2.125 is over 25% of the nozzle exit velocity. The potential core for each jet and the recirculation region where U is negative can be readily identified in Fig. 7.

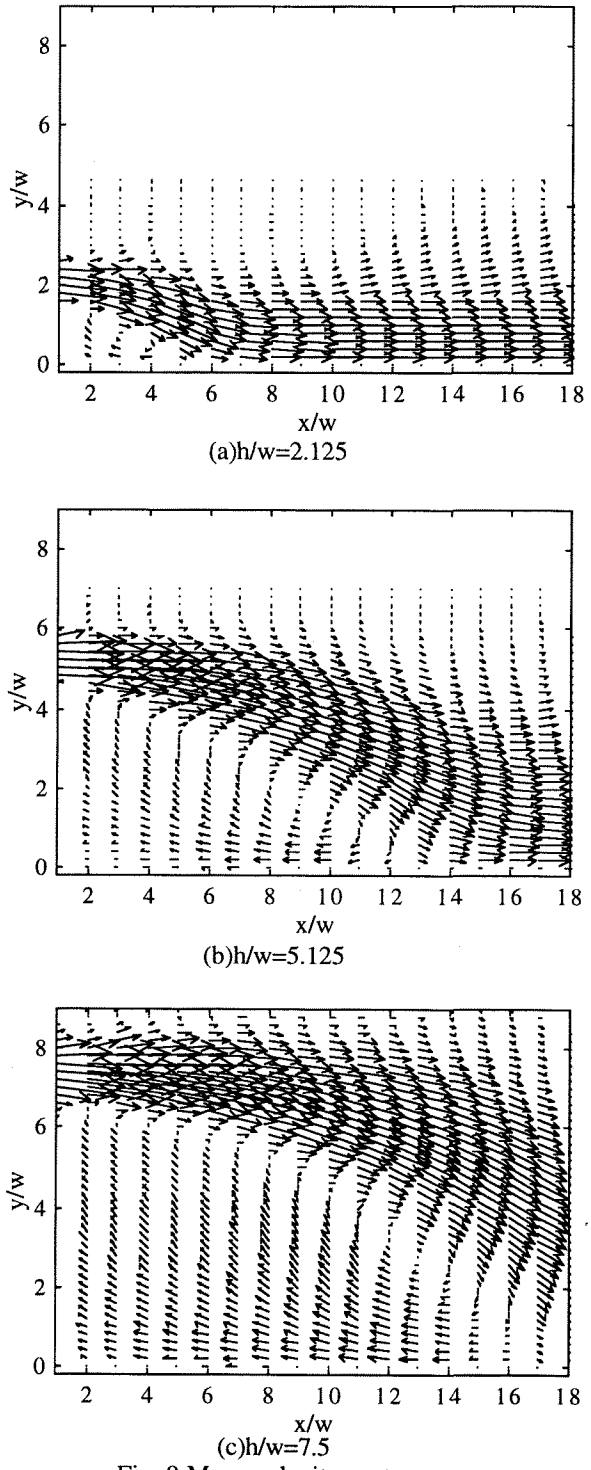

Fig. 9 Mean velocity vectors.

Mean velocity vectors can be constructed from the mean streamwise and lateral velocities profiles shown in Figs. 7 and 8 respectively for the three offset jets. The basic flow features as depicted schematically in Fig. 1 can be identified for all three offset jets in the mean velocity vector field shown in Fig. 9. From the mean velocity vector data, the attachment point for h/w=2.125, 5.125 and 7.5 has been determined to be x_{ip}/w=4.65, 12.5 and 16.5 respectively. Thus the locations of maximum static pressure occur slightly downstream of the attachment point determined from the mean velocity vectors. The differences between x_{ip} and x_{pmax} for h/w=2.125, 5.125 and 7.5 are 1%, 10.4% and 3.6% respectively. The maximum backflow velocity in the recirculation region is approximately 26% of the nozzle exit velocity for all three jets. The locations of the standing vortex centre (x_{vc}/w, y_{vc}/w) for h/w=2.125, 5.125 and 7.5 have been determined to be (3.2,0.7), (9.2,1.8) and (12.4,3.3) respectively. These locations are 68.8%, 73.6% and 75.2% of the distance to the respective attachment point. These results are in reasonable agreement with those of Parameswaran & Alpay [18] who found by flow visualisation technique that the standing vortex centre in their offset jets was approximately 67% of the distance to the attachment point.

As shown in Fig. 10, the attachment lengths determined for the three offset jets in this study are in reasonable agreement with the data in the literature. It should be noted that among the data of Ayukawa & Shakouchi [9], Bourque & Newman [1], Lund [13], Nozaki et al. [10], Pelfrey & Liburdy [14] plotted in Fig. 10, only that of Pelfrey & Liburdy [14] was determined from the mean velocity vector field. A curve of best fit to all the data given in Fig. 10 yields the following expression with a correlation coefficient better than 0.97:

$$x_{ip}/w = 2.630(h/w)^{0.855} \quad \text{for } x/w<20 \qquad (1)$$

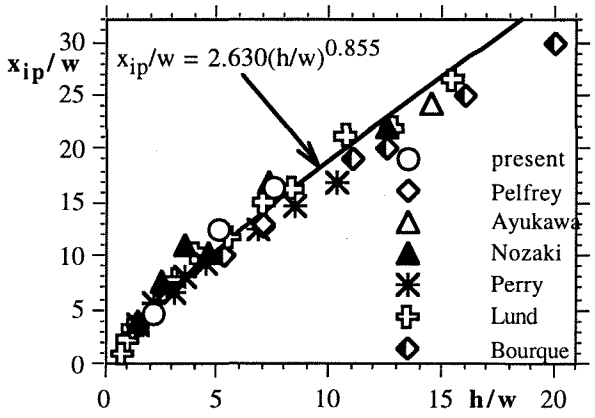

Fig. 10 Variation of attachment lengths with offset ratios.

Maximum streamwise velocity decay and jet half-widths

As shown in Fig. 11, the initial maximum streamwise velocity decay for the three offset jets is faster than that of a single free jet due to the deflection of the jet towards the wall. Furthermore, the initial decay rate decreases as the offset ratio increases because the lateral static pressure gradient decreases with increasing offset

ratio. Downstream of the attachment point, as the static pressure decreases to approach the atmospheric value, the the maximum streamwise velocity increases to a maximum value. Further downstream, the maximum streamwise velocity starts to decay again and its decay rate is expected to approach that of a plane wall jet. However, as shown in Fig. 11, none of the three offset jets has appeared to develop fully into plane wall jets by x/w=28. The offset jet of Pelfrey & Liburdy [14] with offset ratio of 7 has a much faster initial maximum velocity decay compared with the offset jet with offset ratio of 7.5 in this study.

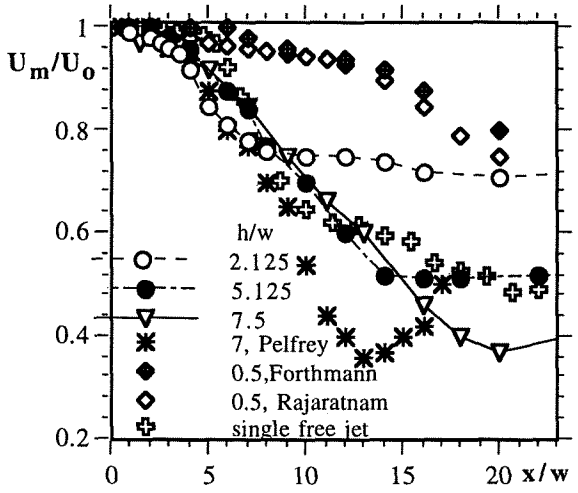

Fig. 11 Maximum streamwise velocity decay for various offset ratios.

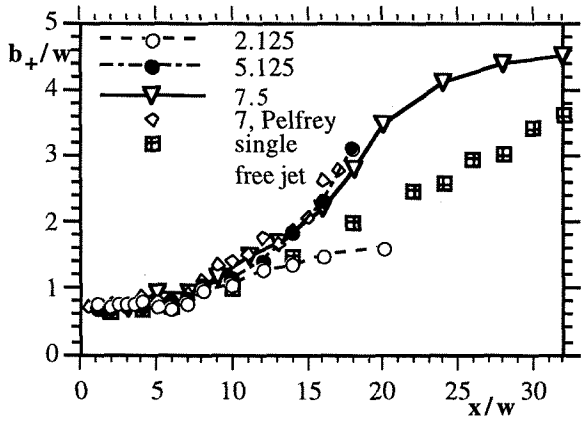

Fig. 12(a) Development of outer shear layer for various offset ratios.

The jet -half widths in the outer and inner shear layers of the three offset jets are shown in Fig. 12(a) and (b) respectively. The initial growth rate of the half-width in the outer shear layer increases with offset ratio. The results of the offset jet of Pelfrey & Liburdy [14] with offset ratio of 7 agree quite well with that of 7.5 in this study. The half-width in the inner shear layer grows immediately downstream of the nozzle, reaches a maximum close to the attachment point and decreases as it develops into a plane wall jet further downstream. The growth of inner shear layer half-width of the jet (h/w=7) of Pelfrey & Liburdy [14] agrees fairly well with the offset jet h/w=7.5; however, it attaches to the wall earlier than that of 7.5 in this study, as has already been observed in Fig. 10.

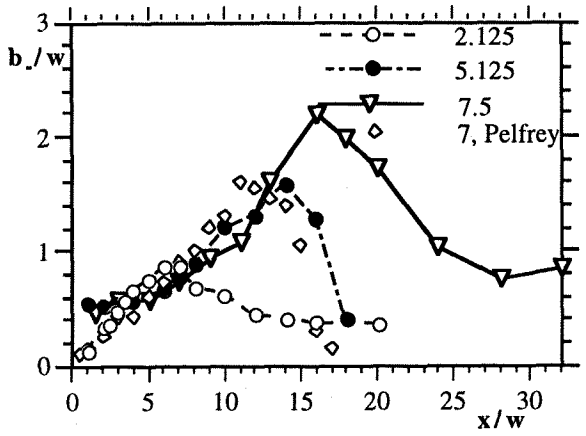

Fig. 12(b) Development of inner shear layer for various offset ratios.

Mean turbulence characteristics

Contours of streamwise turbulence intensities (u'/U_o) for the three offset jets are shown in Fig. 13. Upstream of the attachment point, contours of maximum streamwise turbulence intensities can be seen to be located in the inner and outer shear layers of the jet; these locations also correspond to maximum lateral turbulence intensities (v'/U_o) as shown in Fig. 14. The locations of maximum streamwise turbulence intensity in the inner layer occur in the vicinity of the dividing streamline and immediately upstream of the attachment point (Figs. 13 and 14). These locations also correspond to maximum Reynolds shear stress (Fig. 15), thus indicating strong interactions between the flow in the recirculation zone and the inner shear layer flow of the jet in the vicinity of the attachment point.

Profiles at streamwise locations corresponding to standing vortex centre and attachment point

Profiles of mean streamwise velocities at streamwise locations corresponding to the vortex centre (x_{vc}) and the attachment point (x_{ip}) were obtained by two-dimensional cubic interpolation between measured velocity profiles using MATLAB 4.2c and plotted in Figs. 16(a) and (b) respectively. The velocities are nondimensionalised with reference to the local maximum streamwise velocity (U_m) and the lateral distance from the jet centreline ($y-y_{max}$) is nondimensionalised with respect to the averaged jet halfwidth (b)). Generally speaking, the mean streamwise velocity profiles for each offset jet almost collapse onto each other at both x_{vc} and x_{ip}, thus indicating the suitability of the non-dimensional parameters used.

On the other hand, profiles for streamwise turbulence intensities (u'/U_m) at x_{vc} and x_{ip} as shown in Figs. 17 do not collapse onto each other. While these

profiles have similar shapes and peaks in the inner and outer shear layers are identifiable, they differ significantly in magnitude. These results indicate that while the mean streamwise velocities for various offset ratios when appropriately nondimensionalised display similarity, no such similarity is observed in the turbulence quantities.

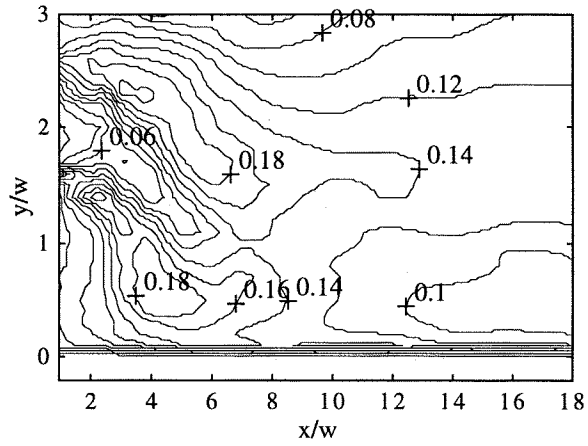

(a) h/w=2.125

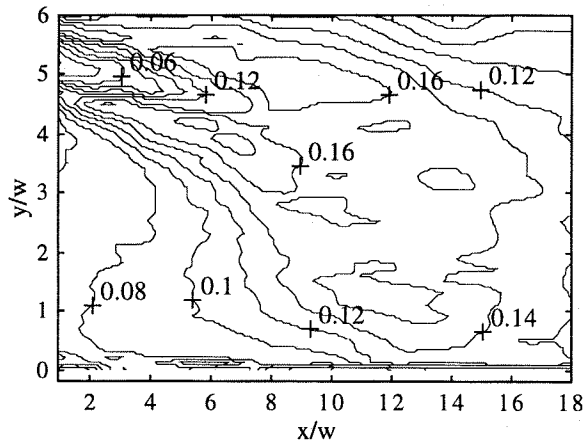

(b) h/w=5.125

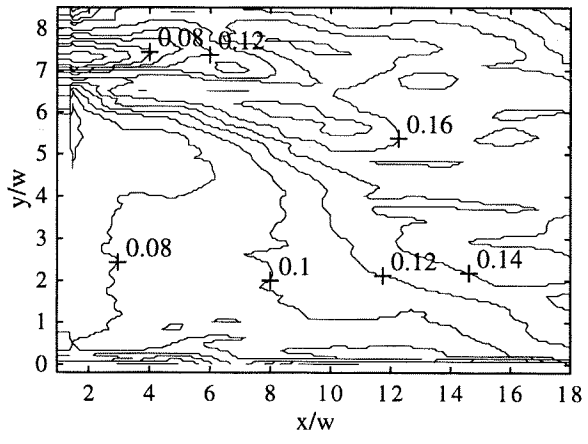

(c) h/w=7.5

Fig. 13 Contours of streamwise turbulence intensities (u'/U_o).

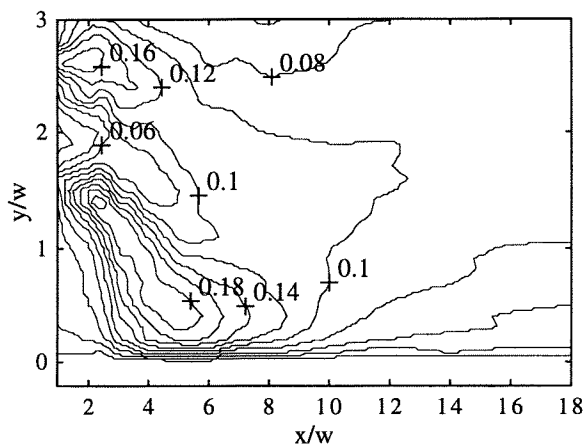

(a) h/w=2.125

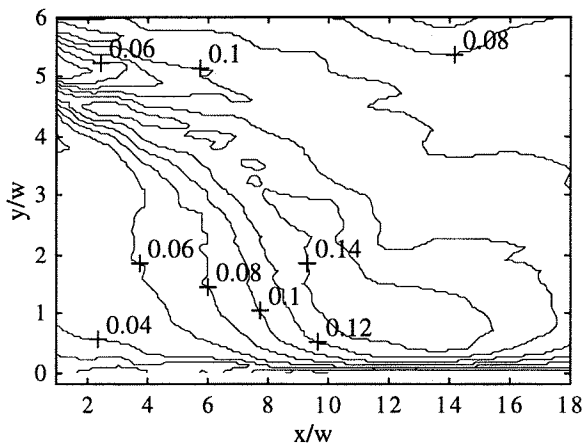

(b) h/w=5.125

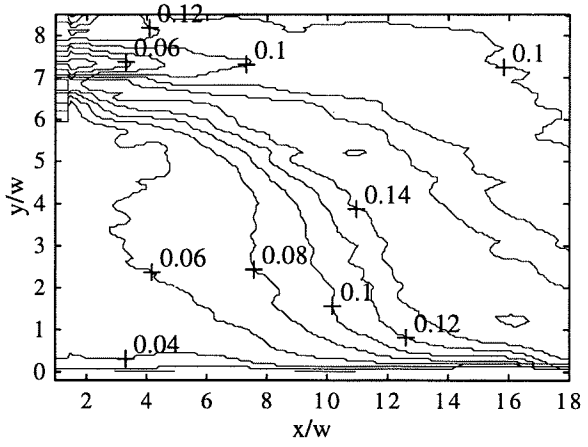

(c) h/w=7.5

Fig.14 Contours of streamwise turbulence intensities (v'/U_o).

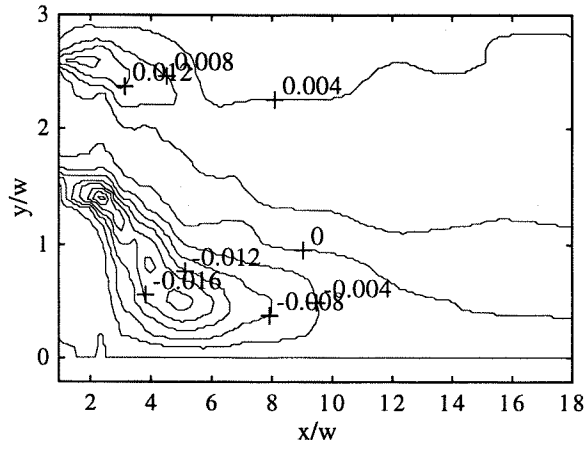

(a) h/w=2.125

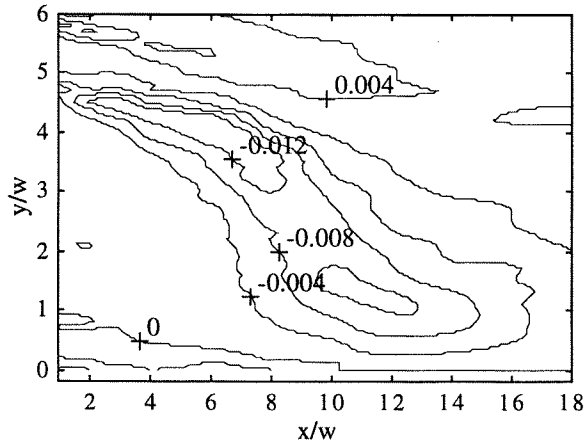

(b) h/w=7.5

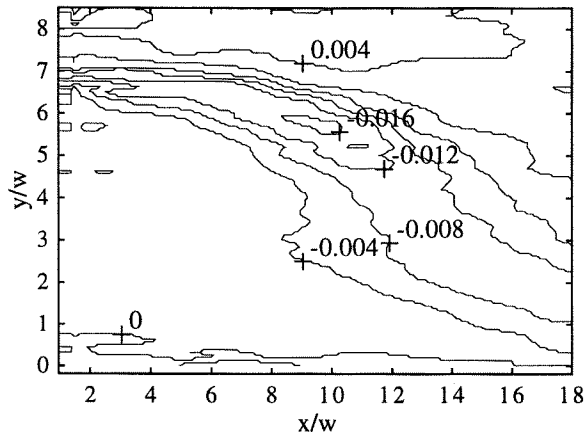

(c) h/w=7.5

Fig.15 Contours of Reynolds shear stress ($\overline{uv}/U_o^2$).

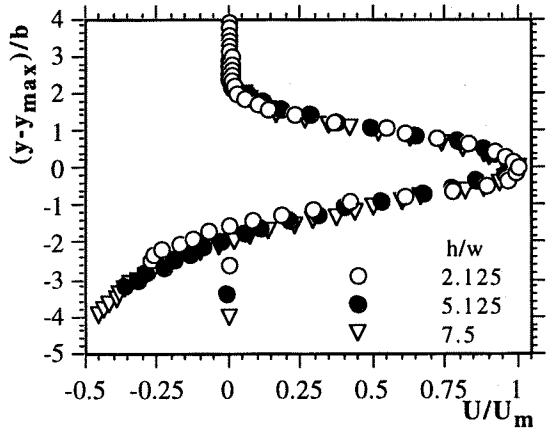

(a) at x_{vc}

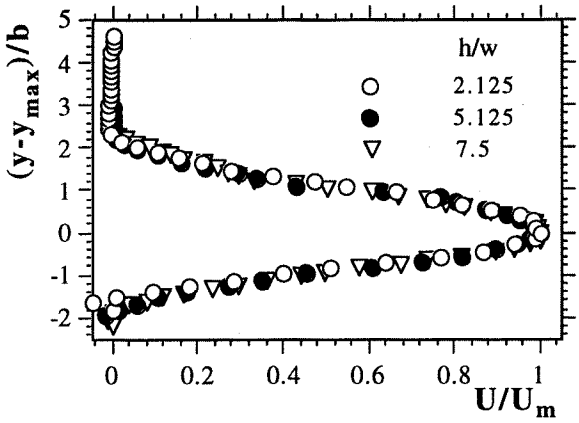

(b) at x_{ip}

Fig. 16 Profiles of nondimensional mean streamwise velocities.

CONCLUSIONS

Static pressure measurements and LDA measurements of a two-dimensional offset jet have been made for three different offset ratios, namely, 2.125, 5.125 and 7.5 at a nozzle exit Reynolds number of 11,000. For h/w=2.125, static pressure profiles show that three dimensional flow effects cannot be neglected unless side plates are installed to prevent entrainment of the surrounding air through the top and bottom sides of the jet. Furthermore, the static pressure variation along the wall for h/w=2.125 has been shown to be independent of the nozzle exit Reynolds number provided that it is greater than 10,000. It has been found that the static pressure gradient and hence the curvature of the jet decreases with increasing offset ratio. Attachment lengths, determined from mean velocity vectors, are in good agreement with data reported in the literature using other techniques such as pressure measurements and flow visualisation. A curve of best fit to the attachment length data indicates that it increases with offset ratio as approximately 4/5th power law. Profiles of mean streamwise velocities, when nondimensionalised by the local maximum (U_m) and the averaged jet halfwidth (b), collapse onto each other for various offset ratios. No

such similarity has been observed for streamwise turbulence intensities.

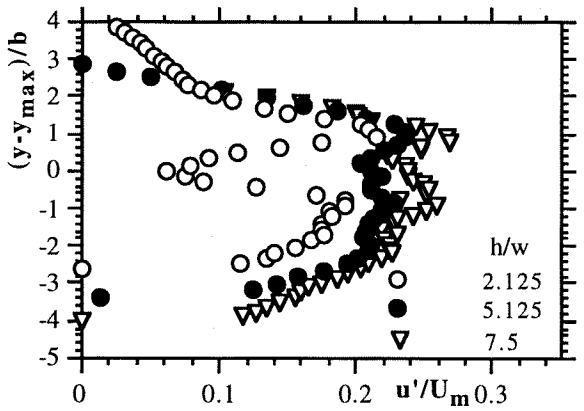

Fig. 17 (a) Profiles of nondimensional streamwise turbulence intensities at x_{vc}.

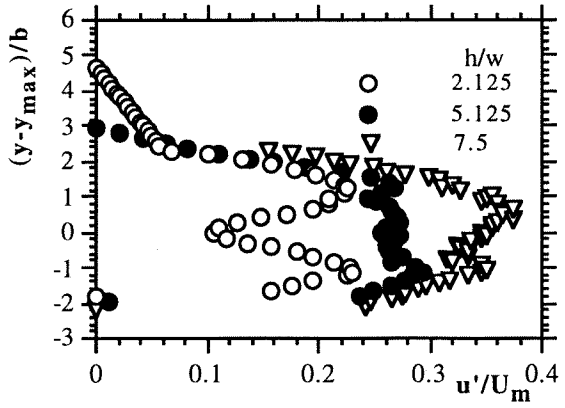

Fig. 17 (b) Profiles of nondimensional streamwise turbulence intensities at x_{ip}.

ACKNOWLEDGMENT

A. Nasr acknowledges receipt of an Iranian Government Scholarship during the course of this work. This project has been supported by the University Rector Special Research Grant.

REFERENCES

1. Bourque C. and Newman B.G. (1960) *Reattachment of a two-dimensional incompressible jet to an adjacent flat plate* The Aeronautical Quarterly,**11**, 201-232. 3. Sawyer R. A., (1960) *The flow due to a two-dimensional jet issuing parallel to a flat plate.* J. Fluid Mech. **9**, 543-561.
2. Newman B. G., (1961), *The Deflection of Plane Jet by Adjacent Boundaries Coanda Effect.* Boundary Layer and Flow control, **1**, 232 - 265.
3. Sawyer R.A. (1960) *The flow due to a two-dimensional jet issuing parallel to a flat plate.* J. Fluid Mech. **9**, 543-561.
4. Sawyer R. A., (1963) *Two-dimensional reattaching jet flows including the effects of curvature on entrainment.* J. Fluid Mech. **17**, 481-498.
5. Bourque C. (1967) *Reattachment of a two dimensional jet to an adjacent flat plate* Advances in Fluidics, ed. by F. T. Brown, ASME, New York, 192-204.
6. McRee D. I. and Moses H. L., (1967)," *The effect of aspect ratio and offset on nozzle flow and entrainment*", Edited by F. T. Brown , ASME Press, New York, pp. 142-161.
7. Perry C. C., (1967) *Two-dimensional jet reattachment.* Advances in Fluidics, ed. by F.T. Brown, ASME, New York, 205-217.
8. Rajaratnam N. and Subramanya N., (1968) *Plane turbulent reattachment wall jets* ASCE J. of Hydraulic Div., **94**, HY1, 95-112.
9. Ayukawa K. and Shakouchi T. (1976) *Analysis of a jet attaching to an offset parallel plate* (1st Report, Oscillation of a jet), Bulletin of the JSME **19**(130), 395-401.
10. Nozaki T., Hatta, K., Nakashima, M. & Matsumura, H. (1979) *Reattachment flow issuing from a finite width nozzle*", Bull. JSME, **22**(165), 340-347.
11. Hoch J. and Jiji L. M. (1981) *Two-dimensional turbulent offset jet-boundary interaction.* Trans. ASME, J. Fluids Eng. **103**, 154-161.
12. Nozaki T., Hatta, K., Sato, N., & Matsumura, H. (1981) *Reattachment flow issuing from a finite width nozzle* (Report 2 - Effects of initial turbulence intensity) Bull. of JSME, **24**(188), 363-369.
13. Lund T. S. (1986) *Augmented thrust and mass flow associated with two-dimensional jet reattachment.* AIAA Journal , **24**(12), 1964-1970.
14. Pelfrey J. R. R. and Liburdy J. A., (1986) *Mean flow characteristics of a turbulent offset jet.* Trans. ASME J. Fluids Eng., **108**, 82-88.
15. Nasr, A. (1995) *Two-parallel plane jets.* PhD thesis, School of Aerospace & Mechanical Engineering, University College, The University of New South Wales.
16. BURSTware 2.00, (1991) *Installation & User's guide."* (C) Dantec Elektronik.
17. Kumada, M., Mabuchi, I. & Oyakawa, K. (1973) *Studies in heat transfer to turbulent jets with adjacent boundaries* (3rd Report, Mass transfer to plane turbulent jet reattached on an offset parallel plate). Bull. of JSME, **16**, 1712-1722.
18. Parameswaran, v. & Alpay, S.A. (1975) *Studies on reattaching wall jets.* Trans. of Canadian Society of Mech. Engr., **3**, 83-89.
19. Forthman, E. (1934) *Uber Turbulente Stranhlausbreitung.* Ing. Arch. **5**, 42.